Angewandte Chemie International Edition

Angewandte International Edition Chemie

How to cite: *Angew. Chem. Int. Ed.* **2026**, e6061192
doi.org/10.1002/anie.6061192

RESEARCH ARTICLE

Potential-Controlled Selective Electrocatalytic Reduction of Nitrite to Four Different Products

Nia J. Harmon[1,2] | Jana Jelušić[1,2] | Jan Paul Menzel[1,2] | Bo Shang[1,2] | Conor L. Rooney[1,2] | Gary W. Brudvig[1,2] | Victor S. Batista[1,2] | Hailiang Wang[1,2]

[1]Department of Chemistry, Yale University, New Haven, Connecticut, USA | [2]Energy Sciences Institute, Yale University, West Haven, Connecticut, USA

Correspondence: Gary W. Brudvig (gary.brudvig@yale.edu) | Victor S. Batista (victor.batista@yale.edu) | Hailiang Wang (hailiang.wang@yale.edu)

Received: 3 June 2026 | **Revised:** 2 August 2026 | **Accepted:** 17 August 2026

Keywords: ammonia | electrocatalysis | hydroxylamine | nitrite reduction | palladium metal | reaction mechanism | surface hydrogen | tunable selectivity

ABSTRACT

We demonstrate for the first time that Pd metal can convert NO_2^- to N_2O, N_2, NH_2OH, and NH_3 in a near-neutral electrolyte, with high selectivity to each product attained by adjusting the applied electrode potential. Notably, N_2 and NH_2OH, which are typically difficult to access, emerge as dominant products. Mechanistic investigation combining computational and experimental studies shows that NO_2^- electroreduction on Pd is controlled by the applied potential and surface coverage of adsorbed H atoms. The interplay of these two factors gives rise to four distinct reaction microenvironments that are consistent with the experimentally observed product distributions. At positive potentials, the pristine Pd surface favors *NO-*NO coupling and N_2O production, whereas at less positive potentials, the same surface with more reducing power favors N_2. At mildly negative potentials, partial H coverage promotes *NO reduction over coupling and leads to NH_2OH production, while at strongly negative potentials, abundant adsorbed H drives complete reduction to NH_3. Together, these studies provide insight into the rich reductive chemistry at Pd active sites under electrochemical control and enable the rational design of Pd catalysts for environmental remediation and sustainable chemical synthesis.

1 | Introduction

The contamination of groundwater and surface water with nitrogen pollutants, including nitrate (NO_3^-) and nitrite (NO_2^-), poses a serious threat to the environment and public health [1–7]. While NO_3^- is typically present at higher concentrations in water than NO_2^-, microorganisms can readily convert NO_3^- into NO_2^-, which is considerably more toxic [3, 4]. The electrochemical reduction of NO_2^- is a promising strategy to address NO_2^- pollution by using renewable electricity to convert NO_2^- into value-added chemicals or harmless nitrogen gas (N_2) under mild reaction conditions [8, 9]. Examples of value-added products generated by NO_2^- electroreduction include ammonia (NH_3), a chemical feedstock for fertilizer production and a potential carbon-free energy carrier; hydroxylamine (NH_2OH), a feedstock for synthetic polymers, pharmaceuticals, and agrochemicals; and nitrous oxide (N_2O), a medical anesthetic [10–14].

The past decade has witnessed the development of many electrocatalysts capable of reducing oxidized nitrogen species (NO_x^{y-}) [8, 9, 15, 16]. The majority of these catalysts generate NH_3, the most reduced form of N among all possible products. The second most common product is N_2O, which can easily accumulate due to its tendency to desorb from most metal surfaces [17]. However, achieving high selectivity toward NH_2OH and N_2 is challenging. NH_2OH is a reactive intermediate that readily undergoes further

Nia J. Harmon and Jana Jelušić contributed equally to this work.

reduction to NH_3, and N_2 formation must compete with reaction pathways leading to NH_3 or N_2O [8, 9, 15, 16]. There are limited reports on heterogeneous electrocatalysts capable of selective NH_2OH or N_2 production [18–25]. For example, Sheng et al. developed boron-doped amorphous bismuth metallene arrays for electrocatalytic NO_3^- reduction in acidic electrolyte, achieving a Faradaic efficiency (FE) of ~85% for NH_2OH at −0.40 V versus the reversible hydrogen electrode (RHE; all potentials in this paper refer to the RHE scale unless otherwise stated) [18]. In another study, Zhou et al. demonstrated the selective electroreduction of nitric oxide (NO) to NH_2OH in a neutral electrolyte using Co single-atom catalysts, with a FE of ~81% at −0.40 V [19]. By comparison, catalysts selective for N_2 are mostly Pd-based. Examples include PdCu and PdAu, which achieve ~90% N_2 selectivity (based on total N mass balance) during NO_3^- or NO_2^- reduction [21–23]. This unique reactivity makes Pd an attractive catalyst for further study. Notably, almost all catalysts for NO_x^{y-} electroreduction target a single product. Thus far, no catalyst has been reported that can generate NH_3, N_2O, NH_2OH, and N_2 with high selectivity.

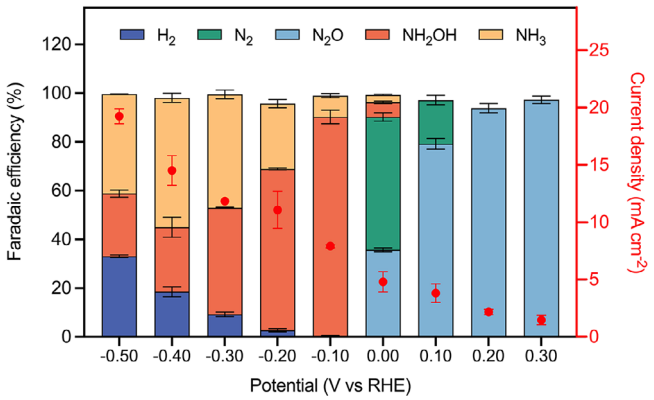

FIGURE 1 | Potential-dependent NO_2^- electroreduction performance of Pd in 0.50 M PB + 0.10 M KNO_2 (pH = 6.8). The error bars represent the standard deviations of at least three independent measurements. Note that some error bars are not visible because they are shorter than the size of the symbol.

In this study, we carefully examine Pd for NO_2^- electroreduction to determine whether it can selectively generate products other than N_2. Interestingly, we find that the product distribution on Pd in 0.50 M phosphate buffer (PB, pH = 6.8) with 0.10 M KNO_2 can be tuned to favor four products: N_2O, N_2, NH_2OH, or NH_3, by simply adjusting the applied electrode potential. Specifically, N_2O is the major product at positive potentials (> 0.00 V), with FEs of ~80%–100%. At 0.00 V, N_2 becomes the major product, with a FE of 55%. NH_2OH is formed at slightly negative potentials (< 0.00 V), achieving a maximum FE of 90% at −0.10 V. NH_3 is also produced under more reducing conditions, becoming the major product at −0.40 V with a peak FE of 53%. Mechanistic investigation suggests that the product distribution is controlled by two key factors: the applied electrode potential (high or low) and the catalyst surface (metallic Pd or Pd hydride, PdH_x), with these four possible combinations giving rise to four different products. Density functional theory (DFT) calculations provide a thermodynamic framework that is consistent with the experimentally observed potential-dependent product distributions by modulating the surface coverage of adsorbed H (*H, where * denotes an adsorbed species). A pristine Pd surface (i.e., with no *H) at high positive potentials thermodynamically favors intermediates leading to N_2O formation, whereas at lower positive potentials the free-energy landscape shifts to thermodynamically favor intermediates along the pathway to N_2. A PdH_x surface with partial *H coverage at moderate negative potentials thermodynamically stabilizes intermediates leading to NH_2OH, whereas increased *H coverage at high negative potentials stabilizes progressively hydrogenated intermediates associated with NH_3 formation.

2 | Results and Discussion

Pd metal was selected for this study because of its unique electrocatalytic properties for small-molecule conversion reactions. For example, Pd can catalyze the electroreduction of carbon dioxide (CO_2) to formate at very low overpotentials [26, 27]. It is also one of the few electrocatalysts capable of reducing NO_x^{y-} to N_2 with high activity and selectivity [28, 29]. The Pd catalyst in this work was prepared by sputter deposition on carbon fiber paper substrates. Scanning electron microscopy reveals an extended material surface with a primary particle size of ~50 nm (Figure S1). X-ray photoelectron spectroscopy analysis confirms the metallic nature of Pd, with Pd $3d_{3/2}$ and $3d_{5/2}$ peaks centered at ~341.4 and ~336.2 eV, respectively (Figure S2) [30]. The Pd 3p spectrum further confirms the presence of metallic Pd, showing $3p_{1/2}$ and $3p_{3/2}$ peaks at ~560.8 and ~533.0 eV, respectively.

To determine the onset potential for NO_2^- reduction on Pd, linear sweep voltammograms (LSVs) were recorded in 0.50 M PB (pH = 6.8), prepared with and without 0.10 M KNO_2 (Figure S3). The onset potential is approximately 0.20 V (Table S1). One-hour controlled-potential electrolysis experiments were then conducted over an applied potential range of 0.30 to −0.50 V. This potential window was selected to drive sufficient, but not excessive, reduction currents for reliable product analysis. The gas-phase products were quantified using gas chromatography, while liquid-phase products were analyzed post-electrolysis using colorimetric methods (Figure S4). Within the applied potential range, the Pd catalyst exhibits clear potential-dependent product selectivity (Figure 1). At low overpotentials, Pd forms products containing two N atoms (N_2-containing products), N_2O and N_2. At high overpotentials, Pd forms products containing one N atom (N_1 products), NH_2OH and NH_3. As the applied electrode potential is decreased from 0.30 to 0.00 V, the N_2O FE decreases substantially from ~100% to 36%, whereas the N_2 FE increases from 0% to 55%. The highest activity and selectivity for N_2O are achieved at 0.20 V, with a total current density of 2.2 mA cm^{-2} and a FE of ~100%. A potential of 0.00 V is optimal for N_2 formation, with a FE of 55%, corresponding to a selectivity of 50% based on total N mass balance, and a total current density of 4.8 mA cm^{-2}. In comparison to other reports (Table S2), this system achieves moderate N_2 selectivity under mild reaction conditions, avoiding highly reducing potentials and strongly acidic or alkaline electrolytes. 0.00 V also marks a turning point in the product distribution, indicating a shift from N_2-containing to N_1 products, with the first detection of NH_2OH (FE ≈ 6%) and NH_3 (FE ≈ 3%). As the electrode potential is decreased from 0.00 to −0.50 V, the FE of NH_2OH increases to a maximum of

90% at −0.10 V, with a total current density of 7.9 mA cm^{-2}, before steadily decreasing. This system exhibits one of the highest reported NH_2OH selectivities while operating at one of the lowest negative potentials and under near-neutral pH conditions (Table S3). Over this potential range, the FE of NH_3 increases to its highest value of 53% at −0.40 V, with a total current density of 14.5 mA cm^{-2}, before competition from hydrogen (H_2) evolution becomes more significant.

The observation of these four different products, all with reasonably high selectivity, is unprecedented and demonstrates that the applied electrode potential enables a high level of control over reaction pathways on Pd surfaces. This behavior highlights a key advantage of this catalyst system over other NO_2^- reduction systems: product selectivity can be tuned simply by changing the electrode potential, without requiring any external modifications to the catalyst, changes to the electrolyte, or adjustments to the reactor configuration. This tunability provides practical versatility, enabling the catalyst to be directed toward N_2 formation for environmental remediation or toward the electrosynthesis of valuable chemical products, such as N_2O, NH_2OH, and NH_3. For example, we leveraged the high activity and selectivity of Pd for NH_2OH production to enable electrosynthesis of oximes from NO_2^- reduction in the presence of carbonyl compounds [31].

The broad product distribution observed on Pd suggests that multiple competing reaction pathways are accessible under electrochemical control. We hypothesize that the interplay of two factors may be responsible for this distinct behavior: 1) a potential-induced transformation of the Pd surface from metallic Pd to PdH_x, and 2) potential-dependent competition between desorption and further reduction of intermediates or products. Pd is known to undergo a transition to PdH_x at approximately 0.00 V [26, 27, 32–34]. This restructuring is easily seen in the cyclic voltammogram measured in H_2SO_4 electrolyte (Figure S5), where PdH_x formation is well documented [32, 33]. More broadly, hydrogen adsorption and PdH_x formation have been observed across a wide range of electrolyte compositions and pH values [27, 35–41]. For example, in electrochemical CO_2 reduction, which is commonly performed in near-neutral electrolytes, metallic Pd at low overpotentials produces formate, whereas PdH_x at higher overpotentials produces CO and H_2 [26, 27, 34]. The transition from Pd to PdH_x is likely responsible for the shift in NO_2^- reduction products from N_2-containing to N_1 products (Figure 1). After NO_2^- is reduced to NO, a critical branching point in the reaction pathway emerges [8, 9]. At low overpotentials, the metallic Pd surface is able to accommodate a high coverage of *NO, under which one *NO can couple with another *NO to form $*N_2O$. In the presence of a sufficiently reducing potential, $*N_2O$ can be further reduced to N_2; otherwise, it may desorb from the electrode surface, resulting in high selectivity toward N_2O [17]. At high overpotentials, increased *H coverage on the PdH_x surface may decrease *NO coverage and promote *NO hydrogenation to *NOH or *NHO, and subsequently to $*NH_2OH$ [42]. Competition between desorption and further hydrogenation determines the relative selectivity between NH_2OH and NH_3.

To test the hypothesis that selectivity is influenced by the competition between coupling, desorption, and further reduction of surface intermediates, we carried out experiments with varied reactant concentrations and electrode potentials. At 0.00 V, as the KNO_2 concentration in the electrolyte is increased from 0.10 to 0.25 M and 0.50 M (see Figures S6–S9 for the corresponding LSVs and calibration curves for product quantification), the combined FE of N_1 products decreases from 9% to 5% and then to 1%, and the N_2 FE decreases from 55% to 31% and then to 23% (Figure 2a). Conversely, the N_2O FE increases from 36% to 64% and then to 76%. Despite the substantial changes in N-containing product selectivity, the total current density increases slightly, from 4.8 mA cm^{-2} to 6.1 mA cm^{-2} and then to 6.4 mA cm^{-2}. Notably, the FE ratio of N_2-containing to N_1 products increases sevenfold with increasing KNO_2 concentration from 0.10 to 0.50 M (Figure 2b), which suggests that higher KNO_2 concentrations favor N-N coupling. This correlation supports our hypothesis that coupling between *NO species leads to the formation of N_2-containing products. At higher NO_2^- concentrations, more *NO accumulates on the Pd surface due to faster reduction of NO_2^-. The resulting increased *NO coverage should promote N-N coupling. Meanwhile, *H coverage is likely reduced under these conditions, which could slow down further reduction of *NO, thereby favoring N_2-containing products and suppressing N_1 products [17, 21, 22].

We also varied the applied electrode potential while fixing the KNO_2 concentration at 0.50 M. As the potential is decreased from 0.00 to −0.10 V and then to −0.20 V, the N_2O FE decreases from 76% to 42% and then to 11% (Figure 2c). The NH_2OH FE increases from less than 1% to 17% and then to 61%, while the NH_3 FE increases from less than 1% to 5% and then to 23%. The N_2 FE, however, follows a volcano-shaped trend, rising from a value of 23% at 0.00 V to a maximum of 37% at −0.10 V before falling to 4% at −0.20 V. The total current density decreases marginally from 6.4 mA cm^{-2} to 6.3 mA cm^{-2} and then to 5.3 mA cm^{-2} over the potential range. The potential-dependent FE ratios of N_2O to N_2 and NH_2OH to NH_3 are plotted in Figure 2d (data are excluded when a product's FE is below 5% due to reliability concerns). The FE ratio of N_2O to N_2 decreases with increasing overpotential, from 3.4 at 0.00 V to 1.2 at −0.10 V, while the FE ratio of NH_2OH to NH_3 decreases from 3.4 at −0.20 V to 2.6 at −0.10 V. These trends suggest that the electrode potential controls the distribution between relatively oxidized and reduced products in both the N_2-containing and N_1 reaction pathways. Taken together, these concentration- and potential-dependent experiments support the mechanistic hypothesis that the competition between coupling, hydrogenation, and desorption of intermediates on the reaction pathway controls the product distribution.

To study the effect of electrolyte pH on Pd-catalyzed NO_2^- reduction, particularly product selectivity, we prepared electrolyte solutions with pH values ranging from 4.0 to 13.7, all containing 0.10 M KNO_2. The corresponding LSVs and calibration curves for product quantification are shown in Figures S10–S17. At pH 4.0, the onset potential for NO_2^- reduction is approximately 0.14 V (Table S1). In this acidic electrolyte, N_2O is the dominant product, maintaining a FE of ~100% from 0.10 to −0.10 V and observed at potentials as low as −0.40 V (Figure 3a). At −0.20 V, NH_2OH and NH_3 emerge for the first time. NH_2OH reaches a maximum FE of 41% at −0.30 V, while NH_3 reaches a peak FE of 8% at −0.40 V. N_2 formation is significantly suppressed, with N_2 first appearing at −0.30 V, where it achieves its highest FE of 8%. As the electrode potential becomes more negative than −0.10 V, H_2 evolution becomes increasingly competitive. At pH 8.5, the onset

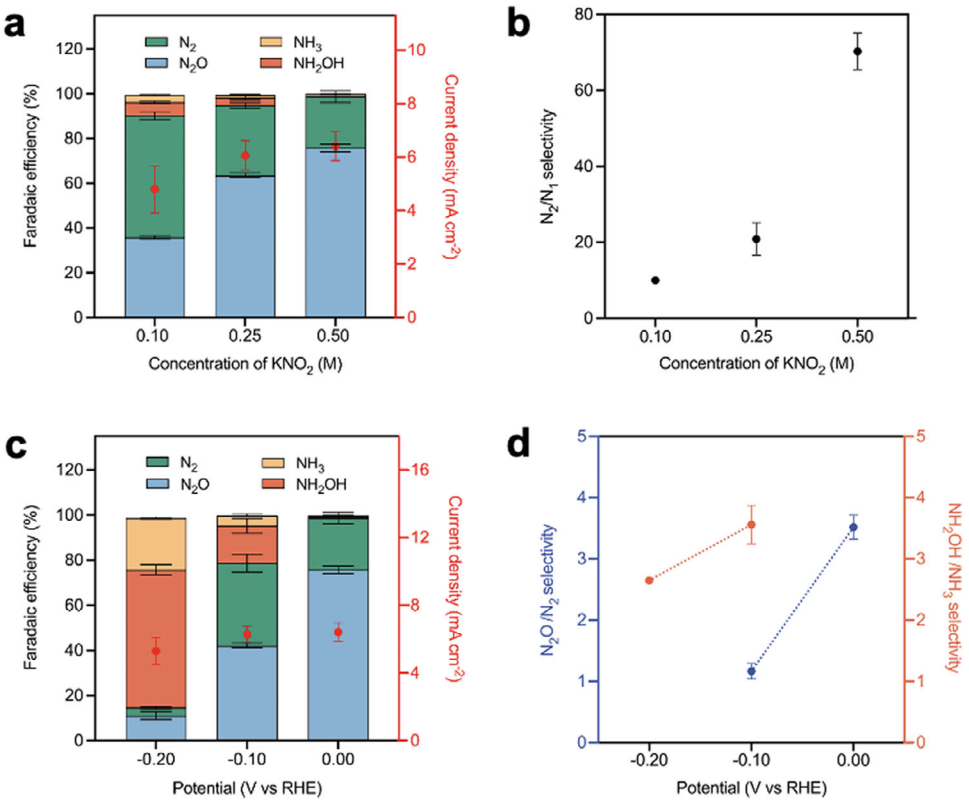

FIGURE 2 | The effect of KNO_2 concentration on the electrochemical NO_2^- reduction performance of Pd. (a) Catalytic performance of Pd at 0.00 V in 0.50 M PB (pH = 6.8) with different concentrations of KNO_2. (b) Effect of KNO_2 concentration on the FE ratio of N_2-containing to N_1 products in 0.50 M PB at 0.00 V. (c) Potential-dependent catalytic performance of Pd in 0.50 M PB + 0.50 M KNO_2 (pH = 6.8). (d) Effect of the applied potential on the FE ratio of N_2O to N_2 and the FE ratio of NH_2OH to NH_3 in 0.50 M PB + 0.50 M KNO_2. Note that ratios involving NO_2^- reduction products with FEs below 5% were not included in this plot. The error bars represent the standard deviations of at least three independent measurements; some error bars are not visible because they are shorter than the size of the symbol.

potential for NO_2^- reduction is −0.72 V (Table S1). Within the potential range of −0.73 to −0.88 V, the main NO_2^- reduction product is NH_2OH, reaching a peak FE of 36% at −0.78 V, whereas NH_3 remains consistently low, with FEs of ~2% (Figure 3b). H_2 is a severe side product in this potential range, with FEs higher than 50%. Interestingly, no N_2-containing products are detected. When the electrolyte pH is adjusted to 10.0 and 13.7, the onset potential for NO_2^- reduction shifts to −0.28 and −0.24 V, respectively (Table S1). At both pH values, NH_3 is the predominant N-containing product, while H_2 dominates at high overpotentials (Figure 3c,d). NH_2OH is formed only at pH 10.0, with FEs lower than 5%. Again, no N_2-containing products are observed. These results demonstrate that the product selectivity of electrochemical NO_2^- reduction catalyzed by Pd is highly dependent on the electrolyte pH. N_2O and N_2 can only be formed under acidic or neutral conditions. The dominant N_1 product switches from NH_2OH to NH_3 at pH values between 8.5 and 10.0. In addition, H_2 evolution is a considerable side reaction at all potentials when the pH is 8.5 or higher. While a detailed mechanistic explanation is beyond the scope of the present study, the relatively low overpotentials under acidic and near-neutral conditions may favor the formation of N_2-containing products, whereas the higher overpotentials required under alkaline conditions may promote the further reduction of NH_2OH, a known intermediate in the reduction pathway to NH_3, rather than its accumulation in the electrolyte [43, 44].

To gain more insight into the potential-regulated product selectivity of NO_2^- reduction among N_2O, N_2, NH_2OH, and NH_3 on Pd surfaces under near-neutral conditions, DFT calculations were employed. Overall, the calculations reveal that the applied electrode potential influences the adsorption of H atoms and modulates the thermodynamic stability of surface intermediates (Figure S18). The intermediates involved, along with the energetics of the reaction pathways, are shown in Figures 4 and 5. The free energies of reactants, intermediates, and products are provided in Table S4.

At more positive potentials, such as 0.30 V, the Pd surface is free of *H and remains pristine (Figure 4a). Under these conditions, the first step of the mechanism involves the dissociation of nitrous acid (HNO_2) to form a proton (H^+) and NO_2^-, with NO_2^- binding to the Pd surface through the N atom. The N—O bond in NO_2^- then cleaves, forming *NO. The dissociated O and H^+ combine to form hydroxide (OH), which is co-adsorbed on the surface. Through subsequent proton-coupled electron transfer (PCET), *OH is hydrogenated to form H_2O, after which H_2O desorbs from the catalyst surface. The calculations indicate that the remaining *NO species is highly stable due to the coordination of the N atom to three Pd atoms and is therefore unlikely to desorb (Figure S19). Because the applied potential is not sufficiently reducing, *NO remains thermodynamically favored relative to *NOH and instead binds to all available valleys on the surface, which results

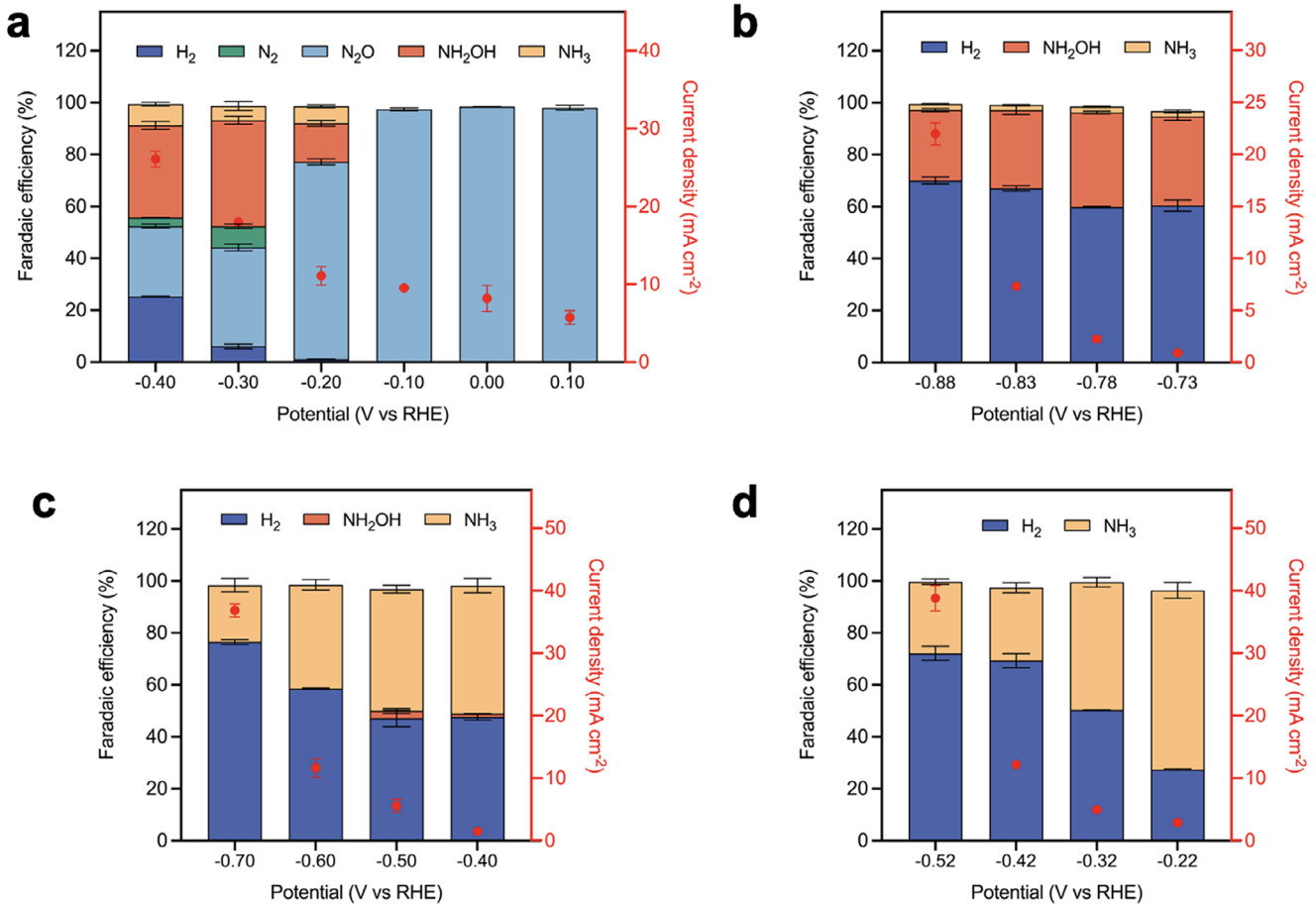

FIGURE 3 | The effect of pH on the electrochemical NO_2^- reduction performance of Pd. Potential dependence study in (a) 0.50 M PB + 0.10 M KNO_2 (adjusted to pH 4.0 using H_3PO_4), (b) 0.50 M $KHCO_3$ + 0.10 M KNO_2 (pH = 8.5), (c) 0.50 M KOH + 0.10 M KNO_2 (adjusted to pH 10.0 using H_2SO_4), and (d) 0.50 M KOH + 0.10 M KNO_2 (pH = 13.7). The error bars represent the standard deviations of at least three independent measurements. Note that some error bars are not visible because they are shorter than the size of the symbol.

in surface poisoning. Complete coverage of the Pd surface by *NO brings neighboring *NO species into close enough proximity for *NO-*NO coupling to form N_2O. The N_2O then desorbs, leaving behind an O atom and a free site on the surface. This reaction is favorable because it relieves surface stress associated with high *NO coverage and generates new free active sites. Reduction of the remaining *O to form H_2O is highly favorable, even at positive potentials, resulting in two free sites that enable HNO_2 dissociation and complete the catalytic cycle.

At a less positive potential (0.00 V), the Pd surface is modeled without any *H (Figure 4b). Same as the N_2O reaction pathway, HNO_2 is reduced via several steps to give *NO on the surface. Then a PCET step reduces *NO at the O atom to form *NOH. Due to the low surface coverage of *H and the limited driving force of the applied potential, *NOH decomposes into *N and *OH before further reduction can take place. Next, PCET converts *OH to H_2O, which desorbs from the surface, leaving *N behind. Repeating this sequence of steps leads to the accumulation of *N on the surface. The *N species can then couple to form N_2, which readily desorbs. This reaction pathway is one of the two dominant mechanisms for N_2 formation at this potential, and has been highly debated in the literature [17, 45–47]. Some studies support the coupling between *N species, while others suggest that N_2O is an intermediate that is reduced to N_2. In this alternative N_2O-mediated pathway, *N can react with HNO_2 to produce N_2O. N_2O is then favorably reduced to $*N_2$ and *O, as shown in the following equation:

$$*N + HNO_2 \xrightarrow[-H_2O]{+H^+ + e^-} *N_2O \quad \Delta G = -1.63\ \text{eV}$$

$$*N_2O \rightarrow *N_2 + *O \quad \Delta G = -1.30\ \text{eV}$$

To investigate the N_2O-mediated pathway experimentally, we performed electrochemical reduction of N_2O in 0.5 M PB (pH = 6.8) catalyzed by Pd (Figure S20). Our results show that at −0.10 V, N_2 is selectively produced, which provides evidence to support the N_2O-mediated pathway. However, despite no direct experimental evidence, the *N-*N coupling pathway cannot be entirely ruled out.

Under moderately negative potentials, such as −0.10 to −0.40 V, calculations indicate that H atom adsorption is energetically favorable (Figure S21). To represent low H coverage, the Pd surface is modeled with a single *H (Figure 5a). As in the previously discussed mechanisms, the reaction begins with HNO_2

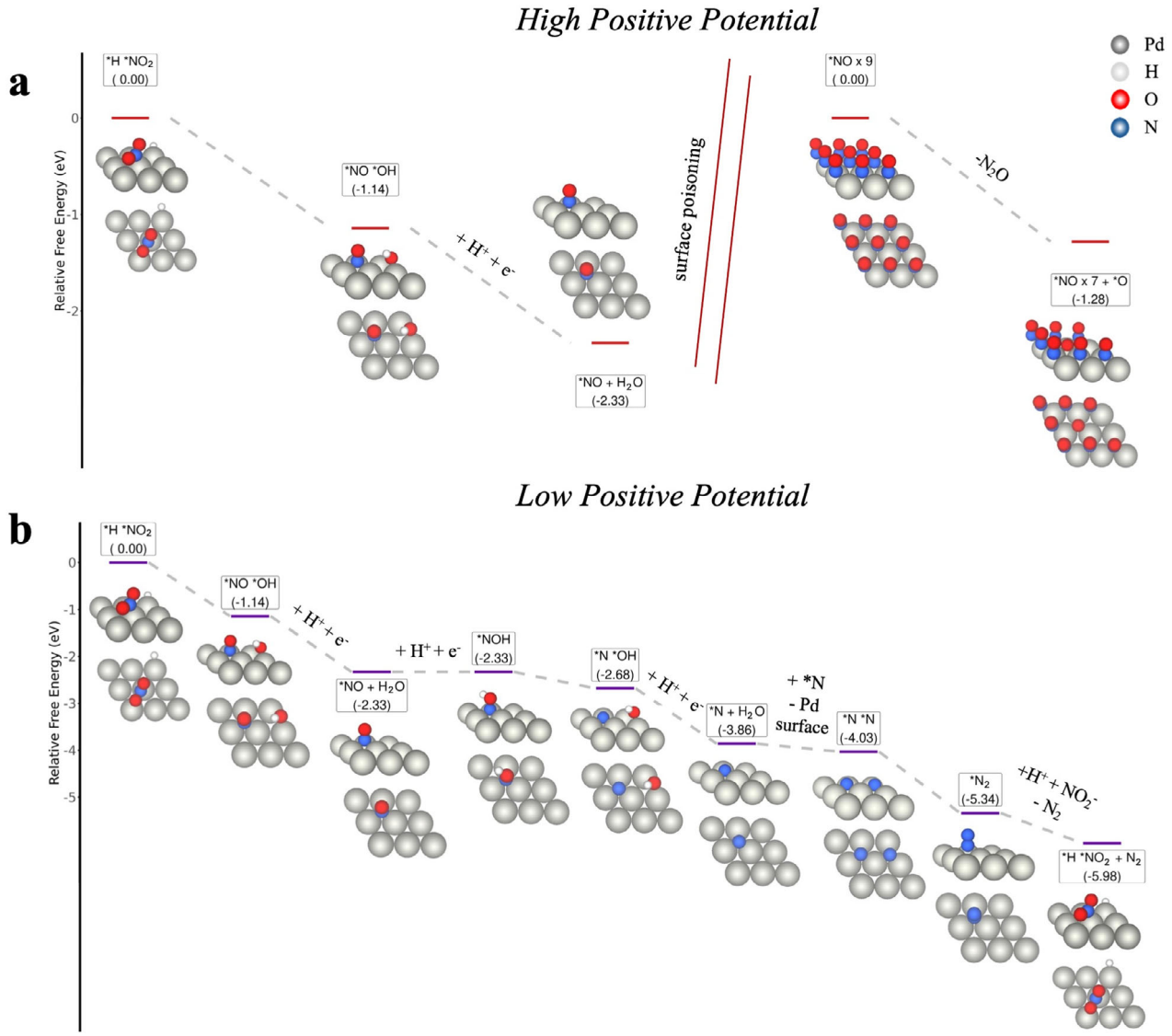

FIGURE 4 | Calculated reaction pathways for electrochemical NO_2^- reduction to N_2-containing products catalyzed by Pd. Free energy profiles are shown for (a) N_2O formation at a positive potential, such as 0.30 V, and (b) N_2 formation at 0.00 V. For both pathways, DFT-optimized structures and reaction equations for each elementary step of NO_2^- reduction on a pristine Pd surface are shown. The grey, white, red, and blue spheres represent Pd, H, O, and N atoms, respectively. Upper graphics show side views, and lower graphics show top views.

dissociation and N—O bond cleavage, producing *NO and *OH, followed by PCET-driven hydrogenation of *OH to H_2O. After H_2O desorbs from the catalyst surface, the applied potential drives PCET to convert *NO to *NOH. The applied potential and the presence of *H thermodynamically favor formation of *NHOH over *NOH dissociation. This reduction step also changes the N binding configuration: in *NOH, N is coordinated to three Pd atoms in a valley configuration, whereas in *NHOH, N binds to two Pd atoms in a bridge configuration. Following this, another PCET step reduces the N atom in *NHOH to *NH_2OH, with N now coordinated to a single Pd atom at a top site. The favorable desorption of NH_2OH allows for additional HNO_2 adsorption.

Finally, at more negative potentials, such as −0.40 to −0.50 V, the Pd surface exhibits high *H coverage. We model this regime by placing H atoms in nearly all valleys of the upper surface, leaving two vacant active sites necessary for HNO_2 dissociation and N—O bond cleavage to *NO and *OH (Figure 5b). Calculations show that NO adsorption at edge sites is energetically less favorable compared to valley sites (Figure S19). Once *NOH forms, two successive reduction steps generate *NH_2OH. Due to the high applied potential, further reduction at the O atom becomes thermodynamically more favorable than NH_2OH desorption, leading to H_2O release and leaving *NH_2. Subsequent reduction of *NH_2 produces *NH_3, which desorbs from the surface with the help of an incoming HNO_2, completing the catalytic cycle.

These calculations reveal how the applied electrode potential, together with potential-dependent *H coverage on the Pd surface, controls product selectivity in NO_2^- reduction. At positive potentials, where there is no *H on the catalyst surface, *NO coverage is high, and *NO-*NO coupling is favored, forming N_2O. At less positive potentials, *H coverage is essentially zero, and while *N-*N coupling is one pathway to N_2 production, there is also sufficient driving force for the reduction of *N_2O to N_2. At slightly negative potentials, *NO is reduced to *NOH. Moderate

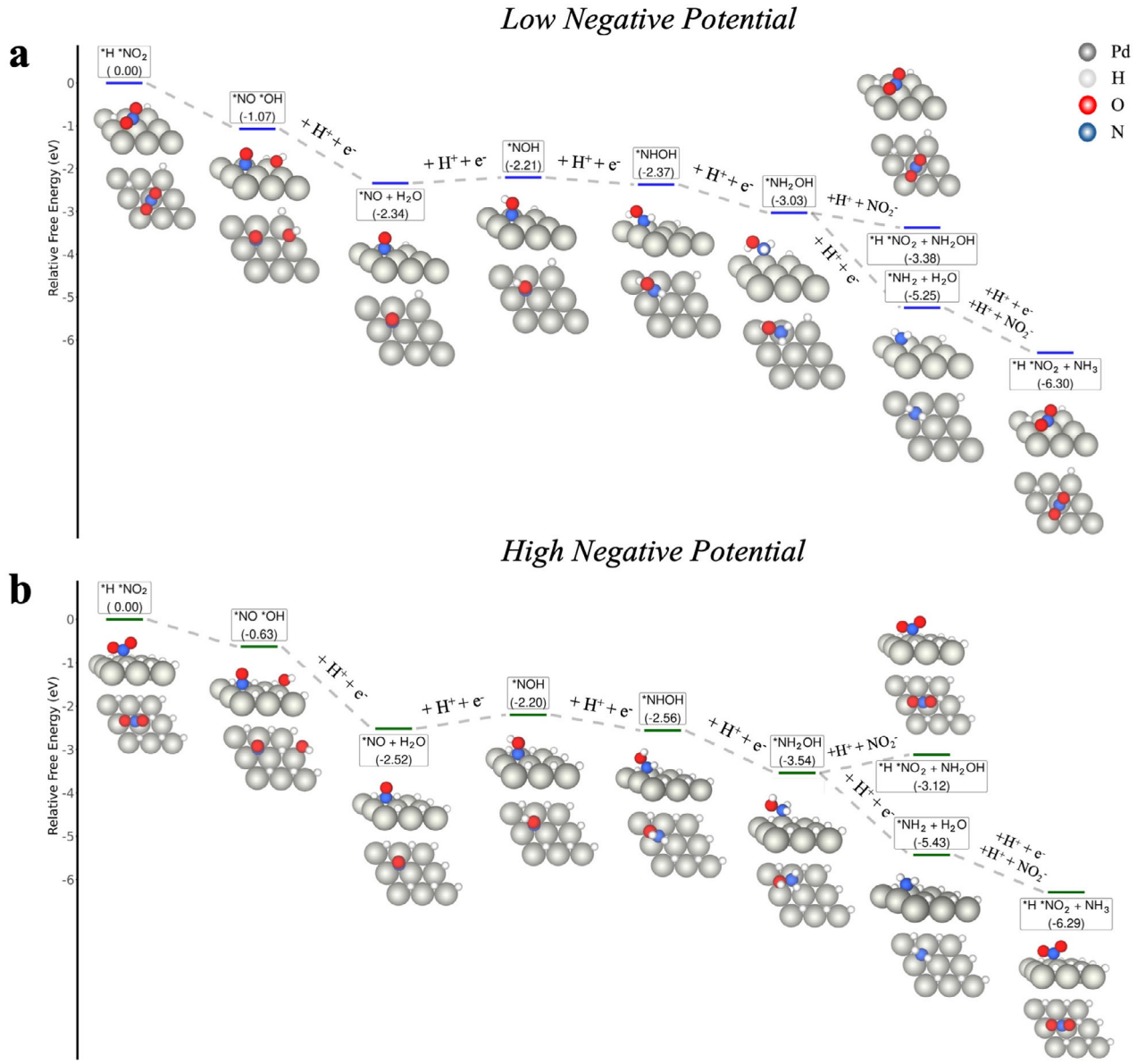

FIGURE 5 | Calculated reaction pathways for electrochemical NO_2^- reduction to N_1 products catalyzed by Pd. Free energy profiles are shown for (a) NH_2OH formation at a low negative potential, such as −0.10 V, and (b) NH_3 formation at a high negative potential, such as −0.50 V. DFT-optimized structures and reaction equations for each elementary step of NO_2^- reduction on a Pd surface with (a) a single *H and (b) high *H coverage are shown. The grey, white, red, and blue spheres represent Pd, H, O, and N atoms, respectively. Upper graphics show side views, and lower graphics show top views.

*H coverage enables *NOH to undergo successive reductions to form NH_2OH, whereas, at more negative potentials, abundant *H thermodynamically favors further hydrogenation of *NOH to NH_3. Overall, our DFT calculations agree with experimental observations across the full potential range.

3 | Conclusion

Metallic Pd exhibits tunable selectivity for NO_2^- electroreduction to N_2O, N_2, NH_2OH, and NH_3 in a near-neutral aqueous electrolyte. This unique potential-dependent product selectivity, achieved without changing the catalyst material or reaction conditions, is governed by the interplay between the reduction potential and the catalyst surface. Positive potentials favor *NO accumulation and N_2O production on a pristine Pd surface, whereas less positive potentials favor N_2 formation on the same surface, possibly via N_2O reduction. Slightly negative potentials introduce moderate *H coverage on the Pd surface that promotes NH_2OH production, while highly negative potentials drive further reduction of NH_2OH to NH_3. These findings highlight the promise of our Pd catalyst system for water treatment and waste valorization via selective NO_2^- conversion to benign or value-added products.

Author Contributions

Nia J. Harmon: conceptualization, investigation, writing – original draft. **Jana Jelušić**: conceptualization, investigation, writing – original draft. **Jan Paul Menzel**: investigation. **Bo Shang**: investigation. **Conor**

L. Rooney: investigation. **Gary W. Brudvig**: writing – review and editing, supervision. **Victor S. Batista**: supervision. **Hailiang Wang**: conceptualization, writing – review and editing, supervision.

Acknowledgments

The experimental work is supported by the U.S. National Science Foundation (CHE-2154724). The computational work is supported by the U.S. Department of Energy, Chemical Sciences, Geosciences, and Biosciences Division, 766 Office of Basic Energy Sciences, Office of Science (Grant DE767 FG02-07ER15909). N.J.H. acknowledges the U.S. National Science Foundation Graduate Research Fellowship.

Conflicts of Interest

The authors declare no conflicts of interest.

Data Availability Statement

The data that support the findings of this study are available from the corresponding author upon reasonable request.

References

1. R. F. Follett and J. L. Hatfield, "Nitrogen in the Environment: Sources, Problems, and Management," *Scientific World Journal* 1, no. 2 (2001): 920–926, https://doi.org/10.1100/tsw.2001.269.

2. J. N. Galloway, J. D. Aber, J. W. Erisman, et al., "The Nitrogen Cascade," *Bioscience* 53, no. 4 (2003): 341–356, https://doi.org/10.1641/0006-3568(2003)053[0341:tnc]2.0.co;2.

3. National Research Council. *Nitrate and Nitrite in Drinking Water* (National Academies Press, 1995), https://doi.org/10.17226/9038.

4. M. H. Ward, T. M. deKok, P. Levallois, et al., "Workgroup Report: Drinking-Water Nitrate and Health—Recent Findings and Research Needs," *Environmental Health Perspectives* 113, no. 11 (2005): 1607–1614, https://doi.org/10.1289/ehp.8043.

5. R. Picetti, M. Deeney, S. Pastorino, et al., "Nitrate and Nitrite Contamination in Drinking Water and Cancer Risk: A Systematic Review With Meta-Analysis," *Environmental Research* 210 (2022): 112988, https://doi.org/10.1016/j.envres.2022.112988.

6. L. Knobeloch, B. Salna, A. Hogan, J. Postle, and H. Anderson, "Blue Babies and Nitrate-Contaminated Well Water," *Environmental Health Perspectives* 108, no. 7 (2000): 675–678, https://doi.org/10.1289/ehp.00108675.

7. P. M. Vitousek, J. D. Aber, R. W. Howarth, et al., "Human Alteration of the Global Nitrogen Cycle: Sources and Consequences," *Ecological Applications* 7, no. 3: 737–750, https://doi.org/10.1890/1051-0761(1997)007[0737:HAOTGN]2.0.CO;2.

8. M. Duca and M. T. M. Koper, "Powering Denitrification: The Perspectives of Electrocatalytic Nitrate Reduction," *Energy & Environmental Science* 5, no. 12 (2012): 9726, https://doi.org/10.1039/c2ee23062c.

9. Z. Wang, D. Richards, and N. Singh, "Recent Discoveries in the Reaction Mechanism of Heterogeneous Electrocatalytic Nitrate Reduction," *Catalysis Science & Technology* 11, no. 3 (2021): 705–725, https://doi.org/10.1039/d0cy02025g.

10. G. Qing, R. Ghazfar, S. T. Jackowski, et al., "Recent Advances and Challenges of Electrocatalytic N_2 Reduction to Ammonia," *Chemical Reviews* 120, no. 12 (2020): 5437–5516, https://doi.org/10.1021/acs.chemrev.9b00659.

11. M. Tawalbeh, S. Z. M. Murtaza, A. Al-Othman, A. H. Alami, K. Singh, and A. G. Olabi, "Ammonia: A Versatile Candidate for the Use in Energy Storage Systems," *Renewable Energy* 194 (2022): 955–977, https://doi.org/10.1016/j.renene.2022.06.015.

12. C. E. Carraher, "Synthesis of Caprolactam and Nylon 6," *Journal of Chemical Education* 55, no. 1 (1978): 51, https://doi.org/10.1021/ed055p51.

13. A. Emmanuel, P. R. Devi, and T. V. Mathew, "Applications of Nitrous Oxide in Food, Plants, and Medicine," *Advances and Technology Development in Greenhouse Gases: Emission, Capture, and Conversion* (Elsevier 2024), 231–244, https://doi.org/10.1016/B978-0-443-19069-8.00008-1.

14. Z. Zafirova, C. Sheehan, and L. Hosseinian, "Update on Nitrous Oxide and Its Use in Anesthesia Practice," *Best Practice & Research Clinical Anaesthesiology* 32, no. 2 (2018): 113–123, https://doi.org/10.1016/j.bpa.2018.06.003.

15. P. H. van Langevelde, I. Katsounaros, and M. T. M. Koper, "Electrocatalytic Nitrate Reduction for Sustainable Ammonia Production," *Joule* 5, no. 2 (2021): 290–294, https://doi.org/10.1016/j.joule.2020.12.025.

16. S. Garcia-Segura, M. Lanzarini-Lopes, K. Hristovski, and P. Westerhoff, "Electrocatalytic Reduction of Nitrate: Fundamentals to Full-Scale Water Treatment Applications," *Applied Catalysis B: Environmental* 236 (2018): 546–568, https://doi.org/10.1016/j.apcatb.2018.05.041.

17. B. H. Ko, B. Hasa, H. Shin, Y. Zhao, and F. Jiao, "Electrochemical Reduction of Gaseous Nitrogen Oxides on Transition Metals at Ambient Conditions," *Journal of the American Chemical Society* 144, no. 3 (2022): 1258–1266, https://doi.org/10.1021/jacs.1c10535.

18. Y. Sheng, H. Chen, J. Geng, et al., "Synergistic Modulation of Intermediate Adsorption and Active Hydrogen Supply Enable Pulsed Nitrate-To-Hydroxylamine Electroreduction With Nearly 100% Faradaic Efficiency," *Angewandte Chemie International Edition* 64, no. 36 (2025): e202509213, https://doi.org/10.1002/anie.202509213.

19. J. Zhou, S. Han, R. Yang, et al., "Linear Adsorption Enables no Selective Electroreduction to Hydroxylamine on Single Co Sites," *Angewandte Chemie International Edition* 62, no. 27 (2023): e202305184, https://doi.org/10.1002/anie.202305184.

20. Y. Li, J. Ge, J. Zhu, et al., "Intermetallic PtSn Nanosheets With P–D Orbital Hybridization for Selective Hydroxylamine Electrosynthesis," *ACS Nano* 19 (2025): 10489–10499, https://doi.org/10.1021/acsnano.5c00544.

21. J. Lim, Y. Chen, D. A. Cullen, S. W. Lee, T. P. Senftle, and M. C. Hatzell, "PdCu Electrocatalysts for Selective Nitrate and Nitrite Reduction to Nitrogen," *ACS Catalysis* 13, no. 1 (2022): 87–98, https://doi.org/10.1021/acscatal.2c04841.

22. J. Lim, D. A. Cullen, E. Stavitski, S. W. Lee, and M. C. Hatzell, "Atomically Ordered PdCu Electrocatalysts for Selective and Stable Electrochemical Nitrate Reduction," *ACS Energy Letters* 8, no. 11 (2023): 4746–4752, https://doi.org/10.1021/acsenergylett.3c01672.

23. H. Li, S. Guo, K. Shin, M. S. Wong, and G. Henkelman, "Design of a Pd–Au Nitrite Reduction Catalyst by Identifying and Optimizing Active Ensembles," *ACS Catalysis* 9, no. 9 (2019): 7957–7966, https://doi.org/10.1021/acscatal.9b02182.

24. M. Dortsiou and G. Kyriacou, "Electrochemical Reduction of Nitrate on Bismuth Cathodes," *Journal of Electroanalytical Chemistry* 630, no. 1-2 (2009): 69–74, https://doi.org/10.1016/j.jelechem.2009.02.019.

25. I. Katsounaros, D. Ipsakis, C. Polatides, and G. Kyriacou, "Efficient Electrochemical Reduction of Nitrate to Nitrogen on Tin Cathode at Very High Cathodic Potentials," *Electrochimica Acta* 52, no. 3 (2006): 1329–1338, https://doi.org/10.1016/j.electacta.2006.07.034.

26. X. Min and M. W. Kanan, "Pd-Catalyzed Electrohydrogenation of Carbon Dioxide to Formate: High Mass Activity at Low Overpotential and Identification of the Deactivation Pathway," 137, no. 14 (2015): 4701–4708, https://doi.org/10.1021/ja511890h.

27. D. Gao, H. Zhou, F. Cai, et al., "Switchable CO_2 Electroreduction via Engineering Active Phases of Pd Nanoparticles," *Nano Research* 10, no. 6 (2017): 2181–2191, https://doi.org/10.1007/s12274-017-1514-6.

28. S. Hörold, T. Tacke, and K. Vorlop, "Catalytical Removal of Nitrate and Nitrite From Drinking Water: 1. Screening for Hydrogenation Catalysts and Influence of Reaction Conditions on Activity and Selectivity," *Environmental Technology* 14, no. 10 (1993): 931–939, https://doi.org/10.1080/09593339309385367.

29. J. Martínez, A. Ortiz, and I. Ortiz, "State-of-The-Art and Perspectives of the Catalytic and Electrocatalytic Reduction of Aqueous Nitrates," *Applied Catalysis B: Environmental* 207 (2017): 42–59, https://doi.org/10.1016/j.apcatb.2017.02.016.

30. D. Briggs, *Handbook of X-Ray Photoelectron Spectroscopy*, ed. C. D. Wanger, W. M. Riggs, L. E. Davis, J. F. Moulder, G. E. Muilenberg (Perkin-Elmer Corp, Eden Prairie, MN, USA, 1981), 3, pp. 190–195.

31. C. L. Rooney, Q. Sun, B. Shang, and H. Wang, "Electrocatalytic Reductive Amination of Aldehydes and Ketones With Aqueous Nitrite," *Journal of the American Chemical Society* 147, no. 11 (2025): 9378–9385, https://doi.org/10.1021/jacs.4c16344.

32. A. Rose, S. Maniguet, R. J. Mathew, C. Slater, J. Yao, and A. E. Russell, "Hydride Phase Formation in Carbon Supported Palladium Nanoparticle Electrodes Investigated Using in Situ EXAFS and XRD," *Physical Chemistry Chemical Physics* 5, no. 15 (2003): 3220, https://doi.org/10.1039/b302956e.

33. A. Czerwiński, I. Kiersztyn, M. Grdeń, and J. Czapla, "The Study of Hydrogen Sorption in Palladium Limited Volume Electrodes (Pd-LVE): I. Acidic Solutions," *Journal of Electroanalytical Chemistry* 471, no. 2 (1999): 190–195, https://doi.org/10.1016/S0022-0728(99)00276-4.

34. A. M. Abdellah, F. Ismail, O. W. Siig, et al., "Impact of Palladium/Palladium Hydride Conversion on Electrochemical CO_2 Reduction via In Situ Transmission Electron Microscopy and Diffraction," *Nature Communications* 15, no. 1 (2024): 938, https://doi.org/10.1038/s41467-024-45096-3.

35. X. Lin, Y. Yang, J. Yang, et al., "In Situ Synthesis of Palladium Hydride as an Efficient and Stable Alkaline Hydrogen Oxidation Reaction Catalyst," *Journal of the American Chemical Society* 147, no. 51 (2025): 47068–47078, https://doi.org/10.1021/jacs.5c12544.

36. P. Zhao, L. Deng, C. Sun, et al., "New Insights Into the Roles of Surface and Lattice Hydrogen in Electrocatalytic Hydrogen Oxidation," *ACS Catalysis* 15, no. 2 (2025): 1352–1362, https://doi.org/10.1021/acscatal.4c06133.

37. X. Min and M. W. Kanan, "PD-Catalyzed Electrohydrogenation of Carbon Dioxide to Formate: High Mass Activity at Low Overpotential and Identification of the Deactivation Pathway," *Journal of the American Chemical Society* 137, no. 14 (2015): 4701–4708, https://doi.org/10.1021/ja511890h.

38. B. M. Tackett, J. H. Lee, and J. G. Chen, "Electrochemical Conversion of CO_2 to Syngas With Palladium-Based Electrocatalysts," *Accounts of Chemical Research* 53, no. 8 (2020): 1535–1544, https://doi.org/10.1021/acs.accounts.0c00277.

39. W. Sheng, S. Kattel, S. Yao, et al., "Electrochemical Reduction of CO_2 to Synthesis Gas With Controlled CO/H_2 Ratios," *Energy & Environmental Science* 10, no. 5 (2017): 1180–1185, https://doi.org/10.1039/c7ee00071e.

40. J. H. Lee, S. Kattel, Z. Jiang, et al., "Tuning the Activity and Selectivity of Electroreduction of CO_2 to Synthesis Gas Using Bimetallic Catalysts," *Nature Communications* 10, no. 1 (2019): 3724, https://doi.org/10.1038/s41467-019-11352-0.

41. J. S. Diercks, J. Herranz, M. Georgi, et al., "Interplay Between Surface-Adsorbed CO and Bulk PD Hydride Under CO_2-Electroreduction Conditions," *ACS Catalysis* 12, no. 17 (2022): 10727–10741, https://doi.org/10.1021/acscatal.2c02660.

42. C. Gu, J. Zhu, X. Kong, and Z. Geng, "Recent Development and Future Perspectives for the Electrosynthesis of Hydroxylamine and Its Derivatives," *Chemical Society Reviews* 54, no. 21 (2025): 10140–10155, https://doi.org/10.1039/d5cs00366k.

43. D. Reyter, D. Bélanger, and L. Roué, "Study of the Electroreduction of Nitrate on Copper in Alkaline Solution," *Electrochimica Acta* 53, no. 20 (2008): 5977–5984, https://doi.org/10.1016/j.electacta.2008.03.048.

44. L. Bai, F. Franco, J. Timoshenko, et al., "Electrocatalytic Nitrate and Nitrite Reduction Toward Ammonia Using Cu_2O Nanocubes: Active Species and Reaction Mechanisms," *Journal of the American Chemical Society* 146, no. 14 (2024): 9665–9678, https://doi.org/10.1021/jacs.3c13288.

45. B. K. Min, Q. Gao, Z. Yan, et al., "Powering the Remediation of the Nitrogen Cycle: Progress and Perspectives of Electrochemical Nitrate Reduction," *Industrial & Engineering Chemistry Research* 60, no. 41 (2021): 14635–14650, https://doi.org/10.1021/acs.iecr.1c03072.

46. A. C. A. de Vooys, M. T. M. Koper, R. A. van Santen, and J. A. R. van Veen, "Mechanistic Study on the Electrocatalytic Reduction of Nitric Oxide on Transition-Metal Electrodes," *Journal of Catalysis* 202, no. 2 (2001): 387–394, https://doi.org/10.1006/jcat.2001.3275.

47. C. Fu, S. Shu, L. Hu, et al., "Electrocatalytic Nitrate Reduction on Bimetallic Palladium-Copper Nanowires: Key Surface Structure for Selective Dinitrogen Formation," *Chemical Engineering Journal* 435 (2022): 134969, https://doi.org/10.1016/j.cej.2022.134969.

Supporting Information

Additional supporting information can be found online in the Supporting Information section.

Supporting File: anie74472-sup-0001-SuppMat.pdf.